Materials Science and Engineering B 118 (2005) 34–38

www.elsevier.com/locate/mseb

# Dependency of the properties of $Sr_xBi_yTa_2O_9$ thin films on the Sr and Bi stoichiometry

Matteo Viapiana [a, b], Michael Schwitters [a], Dirk J. Wouters [a, *], Herman E. Maes [a, b], Omer Van der Biest [c]

[a] *IMEC vzw, Kapeldreef 75, B-3001 Leuven, Belgium*
[b] *ESAT-INSYS Laboratory, Department of Electrical Engineering, Katholieke Universiteit te Leuven, Kasteelpark Arenberg 10, B-3001 Leuven, Belgium*
[c] *Department of Metallurgy and Applied Materials Engineering (MTM), Katholieke Universiteit te Leuven, Kasteelpark Arenberg 44, B-3001 Leuven, Belgium*

**Abstract**

In this study the properties of ferroelectric SBT thin films crystallized at 700 °C have been investigated as function of the Sr and Bi stoichiometry. A matrix of 130 nm $Sr_xBi_yTa_2O_9$ films with $0.7 \leq x \leq 1.0$ and $2.0 \leq y \leq 2.4$ has been realized by metal-organic spin-on deposition technique on $Pt/IrO_2/Ir/TiAlN/SiO_2/Si$ substrates. Within this composition range, we found that the ferroelectric properties peak into a narrow window of $0.8 \leq x \leq 0.9$ and $y \sim 2.25$ with Pr and Ec of 6.5 μC/cm$^2$ and 50 kV/cm, respectively (at 2.5 V). Outside this composition window, the Pr decreases while the hysteresis loop becomes slanted. For some Sr/Bi-ratios even no ferroelectricity was achieved. 2Ec-tendencies were seen as function of the *x*/*y*-ratios, too. Examination of the microstructure of the films by scanning electron microscopy showed that film grain size increased with decreasing Sr-deficiency and that nucleation increased with increasing Bi-excess. At high Sr-deficiency and low Bi-excess, no complete crystallization of the SBT film occurs. From the film morphology, also different phases can be discriminated. X-ray diffraction analysis showed a strong correlation of the film orientation with the film composition. While our results show a clear correlation of Pr, film grain size and orientation with composition, further investigations are required to clarify the relation of the hysteresis parameters with film orientation.


*Keywords:* Ferroelectric SBT thin films; Crystallization; Spin-coating deposition

## 1. Introduction

Bi-layered materials, as $Sr_1Bi_2Ta_2O_9$ (SBT), are key materials for ferroelectric non-volatile RAM (FeRAM) memory, as they offer high-reliability (fatigue-free, very low retention and imprint) operation [1–3]. Also, material and electric properties are known to be sensitive to composition [4–7]. However, main limitations are limited Pr and high crystallization temperature. To optimize the SBT performance, while minimizing the crystallization temperature, knowledge of the SBT material aspects is a strong requirement. It is mandatory to relate thin film composition, orientation, microstructure and electrical performance, however these different aspects have been only partially correlated so far [4–6]. The aim of this study was to make a comprehensive correlation between all these parameters.

## 2. Experimental

SBT thin films were synthesized varying the Bi content from 2.0 to 2.4 and the Sr content from 0.7 to 1.0. This composition range will be called “nominal range” throughout this paper. To emphasize the observed phenomena, a few extra samples out of this nominal range were made as well.

All thin films were prepared by spin-coating deposition of a metal-organic SBT precursor, obtained by mixing (0.5 M) single-metal precursors [8] to the desired ratio.

* Corresponding author.

0921-5107/$ – see front matter © 2004 Elsevier B.V. All rights reserved.
doi:10.1016/j.mseb.2004.12.042

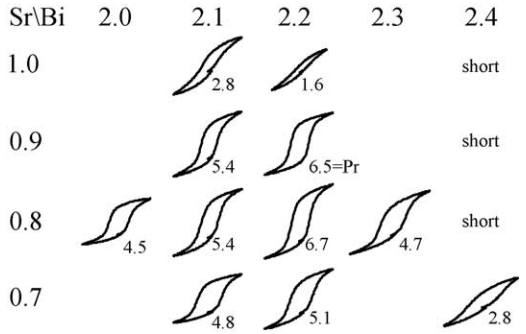


Fig. 1. Hysteresis loop shape and Pr value (expressed in $\mu C/cm^2$) at 2.5 V as function of Sr and Bi composition. Best results are obtained for Sr = 0.8–0.9 and Bi ∼ 2.25.

Films were deposited on Pt electrode substrates ($Pt/IrO_2/Ir/TiAlN/SiO_2/Si$) to perform electrical characterizations and on $SiO_2/Si(1\,0\,0)$ substrate for composition analysis by XRF technique (with estimated errors of 0.02 for Bi- and 0.01 for Sr-content). Spin conditions were 3000 rpm for 30 s, followed by two baking steps on hot plate (160 °C, 1 min and 260 °C, 4 min). For the films on $SiO_2$, a single layer was deposited. The films on Pt electrodes was deposited

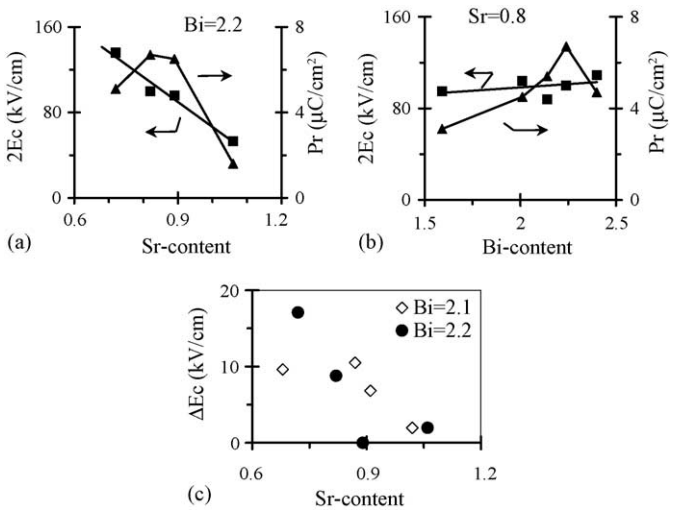


Fig. 2. Variation of Pr and 2Ec as function of (a) Sr composition (at constant Bi = 2.2) and (b) Bi composition (at constant Sr = 0.8). Pr and 2Ec are derived from hysteresis measurements at 2.5 V. (c) The field-offset of the hysteresis loop $\Delta Ec = Ec^+ - Ec^-$ as function of Sr composition.

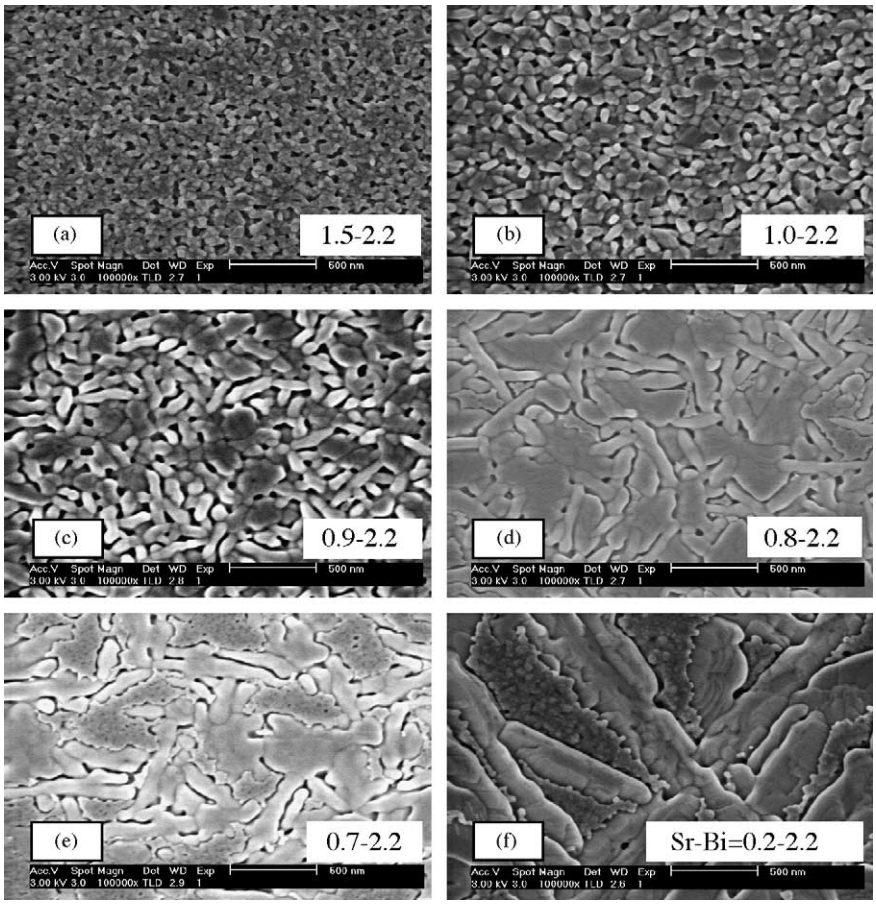


Fig. 3. Secondary electron micrographs revealing the sample grain structure as function of Sr content at fixed Bi = 2.2 (Sr content is decreasing from a to f). In general, we see an increase of grain size (growing into large lamellae) for decreasing Sr content. For the lowest Sr content (f and e), however, "voidy" areas, probably corresponding to a separate phase, can be observed in-between the rod-like grains.

by two layers, with an intermediate anneal at 700 °C, 30 s in $O_2$ by RTP using a heating ramp rate of 40 °C/s. Final crystallization anneal conditions for all samples were 700 °C, 1 h in $O_2$ by RTP with heating rate of 10 °C/s. SBT thickness for the double-layer film on Pt substrates was 130 nm.

Actual film compositions (as determined by XRF on the one-layer films deposited on $SiO_2$) were close to the target conditions, i.e. within an average deviation of 0.05 for both Sr and Bi. In the remainder of the text, we will use the target values for denoting the sample composition.

On the SBT films on Pt substrate, top electrode Pt dots (area = $2.3 \times 10^{-3}$ $cm^2$) were deposited by sputtering through a shadow mask, followed by a top electrode anneal at 700 °C, 10 min by RTP in $O_2$ with heating rate of 10 °C/s.

## 3. Results

Fig. 1 shows the hysteresis performance as function of Sr and Bi composition. The remanent polarization (Pr) shows a maximum of 6.7 μC/$cm^2$ at a composition of Sr = 0.8 and Bi ∼ 2.25. Away from this composition, a Pr decrease together with a slanting of the hysteresis loop is observed. Electrically shorted samples were obtained for Bi ∼ 2.4.

To elucidate the effect of composition, Fig. 2 shows the variation of Pr and the coercive field (2Ec) as function of (a) Sr composition (at constant Bi = 2.2) and (b) Bi composition (at constant Sr = 0.8). Pr shows a rather broad maximum as function of Sr composition while showing a narrow peak as function of Bi composition. This is in good agreement with the results of Bachhofer et al. for MOCVD SBT films [6]. For MOD SBT films Noguchi et al. found a similar dependence on Sr composition, but only a weak dependence on Bi composition was seen [5]. For sol–gel SBT films somewhat different results could be observed at higher anneal temperature of 800 °C especially at larger Sr deficiencies where still an increase in Pr could be observed [4].

In our results, we note that the 2Ec decreases linearly with increasing Sr content, while remaining more or less constant for varying Bi concentrations. For all samples, we note small hysteresis offset ($\Delta Ec = Ec^+ - Ec^-$), which tends to decrease by increasing Sr content (Fig. 2c).

Figs. 3 and 4 reveal the grain microstructure of the different samples. Fig. 3 shows the sample grain structure as

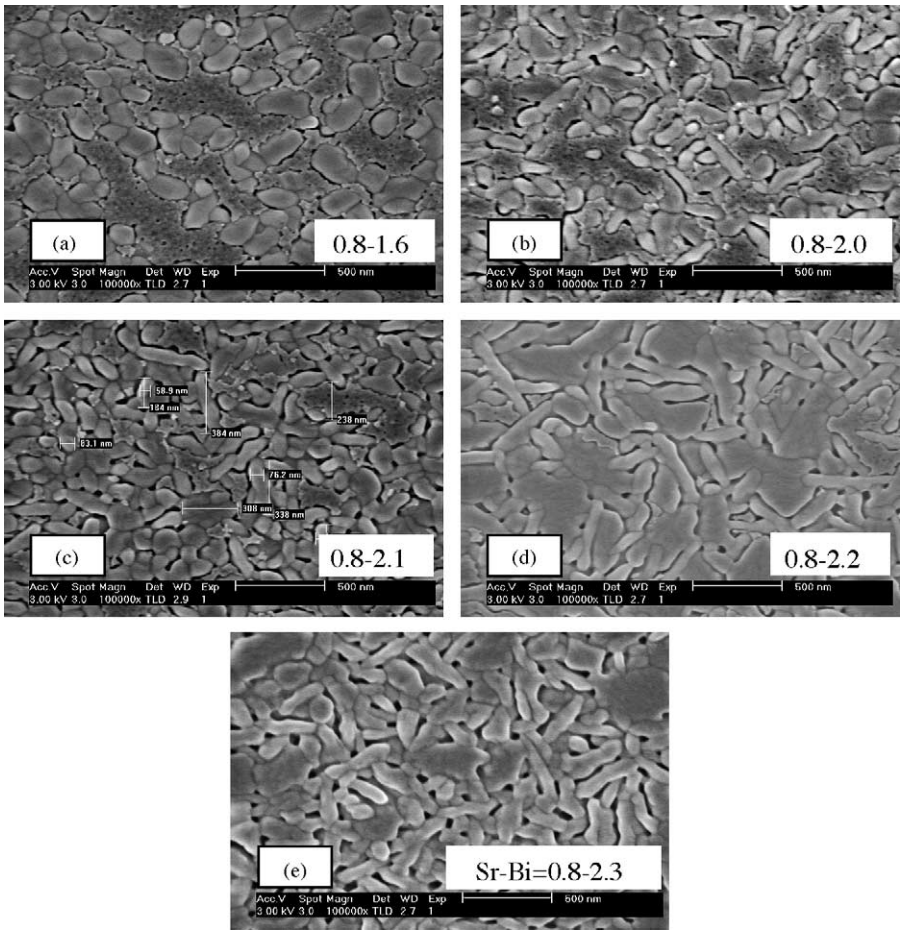


Fig. 4. Secondary electron micrographs revealing the sample grain structure as function of Bi content at fixed Sr = 0.8 (Bi content is increasing from a to e). For the lower Bi content (a–c), we see small grains embedded in a "voidy" area matrix. As Bi content increases, we see and increase of number of grains, while they increase in size (from circular to small lamellae) and the "voidy" areas disappear.

function of Sr content at fixed Bi = 2.2 (Sr content is decreasing from a to f). Two extra samples with compositions out of the nominal range (with Sr = 1.5 and 0.2) help to reveal the phenomena. Their microstructures are represented in Fig. 3a and f. In general, we see an increase of grain size (from ~40 nm small circular grains, growing into large rod-like lamellae up to 1.6 μm long) for decreasing Sr content. For the lowest Sr content (d–f), however, "voidy" areas, probably corresponding to a second phase, can be observed in-between the lamellae-type grains. Cross-section SEM showed that these voids are present throughout the complete film thickness. Note that in [5], similarly, microcrystalline regions and voids were observed in XTEM for low Sr composition.

Fig. 4 shows the sample grain structure as function of Bi content at fixed Sr = 0.8 (Bi content is increasing from a to e). Microstructure in Fig. 4a is associated to a sample with composition out of the nominal window with Bi around 1.6. For the lower Bi content (a–c), we see small grains embedded in what appear as a void-phase matrix. As Bi content increases, we see an increase of number of grains, while they increase in size (from circular to small lamellae) and the voids disappears. This indicates an improved nucleation with increasing Bi content. Fig. 3d and (identical) Fig. 4d show the microstructure associated to sample with the highest Pr-value where Sr/Bi = 0.82/2.24.

Figs. 5–7 show the X-ray diffraction patterns and the effect of composition on the film orientation. For decreasing Sr content at fixed Bi = 2.2, the *c*-axis component (defined as $I(0\,0\,1\,0)/I(1\,1\,5)$ peak intensity ratio) increases while the *a*-axis component (defined as $I(2\,0\,0)/I(1\,1\,5)$) decreases. At increasing Bi content, at fixed Sr = 0.8, *a*-axis component slightly increases while the *c*-axis component shows a small maximum for Bi = 2.2 (estimated error in both graphs is 0.05).

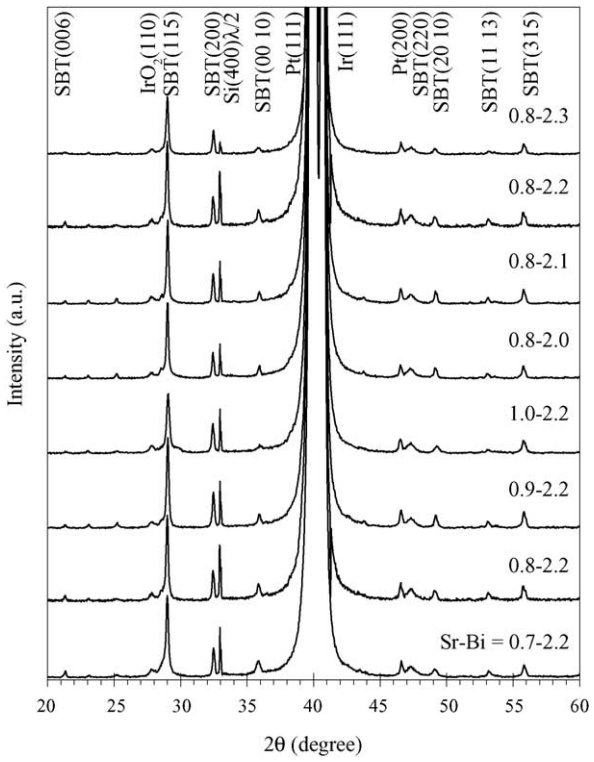


Fig. 5. X-ray diffraction patterns ($\theta$–$2\theta$ scan, Cu $K\alpha_1$) of the thin films at different Sr/Bi-ratio.

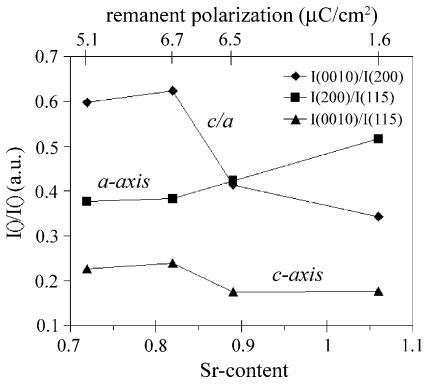


Fig. 6. Film orientation as function of Sr composition at fixed Bi = 2.2. Orientations are quantified by following peak intensity ratio: *a*-axis = $I(2\,0\,0)/I(1\,1\,5)$; *c*-axis = $I(0\,0\,1\,0)/I(1\,1\,5)$; *c*/*a*-axis = $I(0\,0\,1\,0)/I(2\,0\,0)$. The Pr value for the different samples is marked on the secondary *x*-axis. Same trends are observed for Bi = 2.1 (not shown).

Comparing Pr and *c*/*a*-axis ratio (defined as $(I(0\,0\,1\,0)/I(2\,0\,0))$ in both figures, however, no clear correlation can be found. We note that the sample with maximum Pr shows that highest *c*/*a*-axis ratio, but on the other hand other samples with similar Pr can show strongly different *c*/*a*-axis ratio and vice versa.

## 4. Discussion

The evolution of the Pr value with Sr composition may be correlated with the observed microstructure. Starting from high Sr content, we notice first an increase of Pr with decrease

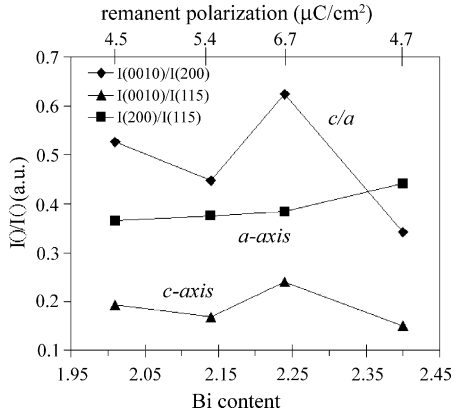


Fig. 7. Film orientation as function of Bi composition at fixed Sr = 0.8. Orientations are quantified by following peak intensity ratio: *a*-axis = $I(2\,0\,0)/I(1\,1\,5)$; *c*-axis = $I(0\,0\,1\,0)/I(1\,1\,5)$; *c*/*a*-axis = $I(0\,0\,1\,0)/I(2\,0\,0)$. The Pr value for the different samples is marked on the secondary *x*-axis. Same trends are observed for Sr = 0.7 and 0.9 (not shown).

in Sr, concomitant with an increase of the grain structure. However, when Sr content is lowered further, the appearance of a separate, probably non-crystallized phase ("voidy" region) becomes visible. The drop of Pr at low Sr contents hence may be attributed to an increased fraction of this secondary phase. The origin of increment of the 2Ec value with decrease of the Sr content seems not related to the microstructure. Only the positive coercive field shifts positively with decreasing Sr content, corresponding to an internal field that may arise from the asymmetric fabrication of top electrode interface.

With increasing Bi content, we observe an increase of the number of grains and a decrease of the non-crystallized phase. Also, at higher Bi content a conglomeration into larger grains is seen. This is concomitant with an increase of the Pr value and less slanted hysteresis shapes. Still, at the highest Bi content, the density of the structure appears to become less dense, what may be reflected in a drop of the Pr for this sample.

In SBT, maximum polarization is aligned to the *a*-axis [6] while *c*-axis oriented SBT crystals have no contribution to the hysteresis [9]. Therefore, the fact that we observe maximal Pr for samples with largest *c*/*a*-axis ratio is not expected. Actually, as samples with similar Pr values may show different *c*/*a* ratio and vice versa, we find there is no clear relation between Pr and *c*/*a* ratio (nonetheless, we see a clear trend of this *c*/*a* ratio with composition). This may indicate that in our films, orientation only plays a secondary role, and e.g. the role of the microstructure is more dominant. Ling et al. obtained similar results, where the 2Pr value was larger on the films with *c*-axis preferred orientation [3]. On the other hand Hendrix et al. proposed a model where also orientation along (1 1 5) plane contributes to the Pr value [10]. Further investigations are required to understand the correlation between Pr value and thin film orientation.

## 5. Conclusions

A composition matrix of SBT thin films has been realized. A clear effect of the *x*/*y*-ratio on different properties (microstructure, orientation and hysteresis characteristics) of the $Sr_xBi_yTa_2O_9$ thin film is found. For FeRAM application, only a narrow film composition range was found applicable. However, while a correlation between film composition, microstructure and Pr value can be found, no correlation of composition Pr and film orientation could be made.

## References

[1] W.-J. Lee, W.-C. Shin, B.-G. Chae, S.-O. Ryu, I.-K. You, S.M. Cho, B.-G. Yu, B.-C. Shin, Integr. Ferro. 46 (2002) 275.
[2] M. Grossmann, O. Lohse, D. Bolten, U. Boettger, R. Waser, W. Hartner, M. Kastner, G. Schindler, Appl. Phys. Lett. 76 (2000) 363.
[3] H. Ling, A. Li, D. Wu, T. Yu, Z. Liu, N. Ming, Integr. Ferro. 47 (2002) 153.
[4] T. Atsuki, N. Soyama, T. Yonezawa, K. Ogi, Jpn. J. Appl. Phys. 34 (1995) 5096.
[5] T. Noguchi, T. Hase, Y. Miyasaka, Jpn. J. Appl. Phys. 35 (1996) 4900.
[6] H. Bachhofer, F. Hintermaier, M. Hauf, O. Spindler, T. Haneder, C. Dehm, H. von Philipsborn, R. Waser, Mater. Res. Soc. Symp. Proc. 596 (2000) 149.
[7] J. Ricote, M.L. Calzada, A. Gonzales, C. Ocal, J. Am. Ceram. Soc. 87 (2004) 143.
[8] Kujundo Chemical Laboratory, Saitama, Japan.
[9] K. Ishikawa, H. Funakubo, Appl. Phys. Lett. 75 (1999) 1970.
[10] B.C. Hendrix, F. Hintermaier, D. Desrochers, J.F. Roeder, T.H. Baum, C. Dehm, N. Nagel, W. Honlein, C. Mazure, Mater. Res. Soc. Symp. Proc. 541 (1999) 275.